AIMS Mathematics, 10(2): 2098–2130.
DOI: 10.3934/math.2025099
Received: 30 September 2024
Revised: 11 December 2024
Accepted: 26 December 2024
Published: 08 February 2025

https://www.aimspress.com/journal/Math

Research article

Numerical study of soliton behavior of generalised Kuramoto-Sivashinsky type equations with Hermite splines

Abdul-Majeed Ayebire[1,2], **Saroj Sahani**[3], **Priyanka**[1,4,*] **and Shelly Arora**[1,*]

[1] Department of Mathematics, Punjabi University, Patiala, Punjab-147002, INDIA
[2] Department of Statistics, Bolgatanga Technical University, Bolgatanga, GHANA
[3] Department of Mathematics, South Asian University, New Delhi-110068, INDIA
[4] Department of Mathematics, Central University of Haryana, Jant-Pali, Mahendargarh, Haryana-123031, INDIA

* **Correspondence:** Email: priyanka_rs@pbi.ac.in; aroshelly@pbi.ac.in.

Abstract: The traveling wave behavior of the nonlinear third and fourth-order advection-diffusion equation has been elaborated. In this study, the effect of dispersion and dissipation processes was mainly analyzed thoroughly. In the thorough analysis, strictly permanent short waves to breaking waves, having comparative higher amplitudes, have been observed. The governed problem was employed with the space-splitting method for a coupled system of equations to conduct the computational process. For the time derivative, the Crank-Nicolson difference approximation was studied. An orthogonal collocation method using Hermite splines has been implemented to approximate the solution of the semi-discretized coupled problem. The proposed method reduces the equation to an iterative scheme of an algebraic system of collocation equations, which reduced the computational complexity. The proposed scheme is found to be unconditionally stable, and the numerical demonstrations and comparisons represented the computational efficiency.

Keywords: Crank-Nicolson technique; collocation scheme; KdV Burger equation; Gardner equation; soliton solution; shock wave
Mathematics Subject Classification: 35B30, 35B35, 35C10, 35B20, 65D07

1. Introduction

Nonlinear higher-order partial differential equations play an essential role in the physical processes occurring in various sciences and engineering disciplines. The fluid dynamical waves in oceanography and bio-fluid dynamics are usually framed by nonlinear higher-order perturbed forms of partial

differential equations. In general, the partial differential problems can be of the form:

$$F(u, u_t, u_\zeta, u_{\zeta\zeta}, ..., \zeta, t) = 0. \tag{1.1}$$

The nonlinear higher-order differential problems have been studied so far with various analytical and numerical techniques. Yet, there is no straightforward technique to thoroughly analyze any family of differential problems. The sub-equation method and the generalized Kudryashov method [1] discussed the soliton-type solutions of evolution equations. The Homotopy analysis J-transformation method is discussed in [2] to analyze the turbulent solutions of the generalized Kuramoto-Sivashinsky equation with the fractional operator. The compact solution is the advantage of any analytic technique but is restricted to specific conditions to study nonlinear differential problems. Various numerical techniques have been designed, such as Legendre wavelets methods [3], a formulation of the fifth order Korteweg-de Vries (KdV) equation in the form of Evans function [4], a rational spectral method [5], mesh-free collocation method [6], etc.

In this study, a prominent position occupying fourth-order nonlinear problems is elaborated on with respect to the perturbation parameter.

$$\underbrace{u_t + \alpha(u)u_\zeta + \delta u_{\zeta\zeta\zeta}}_{\text{KdV}} + \underbrace{\kappa u_{\zeta\zeta} + \varepsilon u_{\zeta\zeta\zeta\zeta}}_{\text{KS}} = 0, \quad (\zeta, t) \in (a, b) \times (0, T]; \tag{1.2}$$

subjected to the initial and boundary data as follows:

$$u(\zeta, 0) = \phi(\zeta); \tag{1.3}$$

$$u(a, t) = \psi_1(t);\ u(b, t) = \psi_2(t); \tag{1.4}$$

$$u_{\zeta\zeta}(a, t) = \psi_3(t);\ u_{\zeta\zeta}(b, t) = \psi_4(t); \tag{1.5}$$

where κ, δ and ε are the known constant coefficients and $\alpha(u)$ represents a function of $u(\zeta, t)$, describing the physical processes. The functions $\phi(\zeta)$ and $\psi_i(t) : i = 1, 2, 3, 4$ are the known continuous functions restricting $u(\zeta, t)$ at initial time and the spatial boundary. For $\delta = 1$ and $\alpha(u) = u$, the equation(1.2) was introduced by Benny in the study of long waves on thin fluid films [7] and is referred to as a special case of the Benny equation. Nowadays, the problem (1.2) has also been studied as the generalized Kuramoto-Shivashinsky equation by the Lattice Boltzmann method [8], collocation method with B-splines functions [9], methods of lines accompanied by radial basis functions [10], moving least square meshless method [11], and the Chebyshev spectral collocation method [12]. The proposed problem has also been considered as the KdV-Burgers-Kuramoto equation in [13] considering the traveling fronts for small dissipation.

The proposed problem exhibits rich solutions ranging from stable short waves to turbulent shock waves, and also has applications in various disciplines like the flow of turbulent air over the laminar fluid [14] and solidification of alloys [15]. A numerical study of flame dynamics and instabilities represented by the Kuramoto-Sivashinsky type equation has been conducted by [16]. A numerical study accounting for the thin film growth and its roughness modeled by the conserved Kuramoto-Sivashinsky equation has been presented in [17]. Earlier, the exact form of solution has been obtained for the aforementioned problem using the Weiss—Tabor—Carnevale method [18]. Various other aspects of the problem, like the existence of the solution, its similar solutions and the structure of the traveling wave solution, and the Gevrey regularity and the stability of the solution, have been discussed

by [19–21]. The evolution of one or more traveling pulses with the dominating dispersion in Eq (1.2) has been described by [22]. Solitary wave solutions due to dissipation as well as instability has been derived by [23]. In higher dimensions, [24], the existence and nonlinear stability of solution for Eq (1.2) have been elaborated. A study using equivalence transformation leading to an algebraic system of equations has also been conducted in [25] for the proposed problem (1.2).

Earlier, various forms of the traveling waves have been studied by researchers regarding the Kuramoto-Sivashinsky (KS) equation [26, 27], KdV equation [28, 29], KdV Burgers equation [30], and Benjamin–Bona–Mahony–Burgers' equation [31] with conservative compact scheme.

The aforementioned problem incorporates the effect of dispersion as well as the dissipation process due to the Kuramoto-Shivashinsky equation. The addition of dispersion($\delta > 0$) changes the time evolution of the wave significantly.

The balancing effect of both the third and fourth-order derivative terms corresponding to the different initial conditions, especially the sech function, is thoroughly elaborated concerning the perturbed parameters. It is observed that as the perturbation parameter $\varepsilon \to 0.5, 0.1$, humps with higher amplitude, yet bounded, and starts to appear due to suppressed dissipative effect only on the negative domain, then for the nonnegative domain, the wave saves its pattern irrespective to the values of ε. Also, the problem was studied with dominant dissipation, where permanent short waves were observed. A detailed study of the dissipation system is found in [32, 33].

In this manuscript, the traveling waves under the influences of dissipation and dispersion are investigated. The rest of the study is manipulated as follows: In Section(2), a weighted finite difference scheme has been studied. Section(3) discusses the fully discretization of the proposed technique. Section(4) comprises the stability analysis using the von Neumann method. The numerical illustrations are presented in Section(5). The conclusion of the entire study is discussed in Section(6).

2. Space splitting and semi discretization technique

In order to meet the requirement that the approximate solution should satisfy the boundary conditions imposed on the solution, the fourth order equation is reduced to a coupled system of second order by assuming a differentiable function $w = -u_{\zeta\zeta}$ [34]. The reduced system reads:

$$\begin{aligned} w &= -u_{\zeta\zeta}; \\ u_t + \alpha(u)u_\zeta - \delta w_\zeta - \kappa w - \varepsilon w_{\zeta\zeta} &= 0. \end{aligned} \tag{2.1}$$

To numerically approximate the solution, the coupled system of equations, after reduction of the order of the proposed problem, is treated with the Crank-Nicholson scheme for time variable coupled with the collocation method for spatial approximation. Earlier, the traveling wave behavior of the Kuramoto-Shivashinsky equation [35], Burgers Huxley and Burgers Fisher [36] and Benjamin-Bona-Mahony-Burgers equations [37], singularly perturbed problems [38], etc. have been studied by the weighted finite difference scheme with quintic Hermite spline collocation method. Here, the simultaneous impact of the dispersive and dissipative mechanisms on the traveling waves and the corresponding perturbed problems have been considered.

In the present study, the Crank-Nicolson (CN) scheme as proposed by [39] operates on the mean of function over the interval $[t_j \;\; t_{j+1}]$ with uniform distribution of points [35, 38].

Define the partition $\pi_t : 0 = t_0 < t_1 < \ldots < t_M = T$ with $\tau = t_{j+1} - t_j$. After applying the CN scheme on the coupled system of equations given by Eq (2.1), following system of equations appears:

$$w^{j+1} + w^j = -u_{\zeta\zeta}^{j+1} - u_{\zeta\zeta}^j; \tag{2.2}$$

$$\frac{u^{j+1} - u^j}{\tau} + \frac{(\alpha(u)u_\zeta)^{j+1} + (\alpha(u)u_\zeta)^j}{2} - \delta\frac{w_\zeta^{j+1} + w_\zeta^j}{2} - \kappa\frac{w^{j+1} + w^j}{2} - \varepsilon\frac{w_{\zeta\zeta}^{j+1} + w_{\zeta\zeta}^j}{2} = 0, \tag{2.3}$$

and the nonlinear function $f(u, u_\zeta)^{j+1} = (\alpha(u)u_\zeta)^{j+1}$ is quasi-linearized with truncation error of order $O(\tau^2)$ by

$$f(u, u_\zeta)^{j+1} \approx \tau\frac{\partial f(u, u_\zeta)^j}{\partial u}u_t(t_j) + \tau\frac{\partial f(u, u_\zeta)^j}{\partial u_\zeta}u_{\zeta_t}(t_j). \tag{2.4}$$

The non-linearity is treated with different formulations using implicit and compact finite difference schemes in [40, 41]. Also, a special case of quasi-linearization of the nonlinear term, i.e., $\alpha(u) = u$, is studied by [42]. After rearranging the terms, the following system is obtained:

$$w^{j+1} + u_{\zeta\zeta}^{j+1} = -w^j - u_{\zeta\zeta}^j; \tag{2.5}$$

$$u^{j+1} + \frac{\tau}{2}\{\alpha(u)^{j+1}u_\zeta^j + \alpha(u)^j u_\zeta^{j+1}\} - \frac{\delta\tau}{2}w_\zeta^{j+1} - \frac{\kappa\tau}{2}w^{j+1} - \frac{\varepsilon\tau}{2}w_{\zeta\zeta}^{j+1} = u^j + \frac{\delta\tau}{2}w_\zeta^j + \frac{\kappa\tau}{2}w^j + \frac{\varepsilon\tau}{2}w_{\zeta\zeta}^j; \quad j = 0, 1, 2, \ldots, M. \tag{2.6}$$

For convenience, write $u(\zeta, t_{j+1}) = u^{j+1}$.

3. Fully discretization technique

Orthogonal splines are the piecewise orthogonal polynomials that interpolate the function at node points. Hermite splines are orthogonal splines and are usually followed to interpolate the function. Earlier, the essence of Hermite splines has been discussed in many ways. Hermite splines are considered to be the extension of the Lagrangian interpolating polynomials. Hermite interpolating polynomials of order $'2k + 1'$ interpolate the function and its k^{th} order derivative at node points. This feature of Hermite interpolating polynomials makes it superior to Lagrangian interpolating polynomials. In the present study, quintic Hermite splines, which are of order 5, are followed. Piecewise, the basis includes six splines and interpolates the function as well as its first and second-order derivatives at intermediate node points. The detailed study of quintic Hermite splines is given hereunder.

Consider an interval $I = [a, b]$, let Π be the partition of I such that:
$\Pi : a = \zeta_0 < \zeta_1 < \zeta_2 < ... < \zeta_{m-1} < \zeta_m = b.$
Let $I_\gamma = [\zeta_{\gamma-1}, \zeta_\gamma]$ such that $\gamma = 1(1)m$ is the γ^{th} subinterval of the partitioned domain. Let $h = \zeta_\gamma - \zeta_{\gamma-1} : 1 \le \gamma \le m$ represent the constant step size of the partition Π. The piecewise interpolating Hermite splines are represented as follows:

$$Q_i(\zeta) = \begin{cases} 6\frac{(\zeta_{i+1}-\zeta)^5}{(\zeta_{i+1}-\zeta_i)^5} - 15\frac{(\zeta_{i+1}-\zeta)^4}{(\zeta_{i+1}-\zeta_i)^4} + 10\frac{(\zeta_{i+1}-\zeta)^3}{(\zeta_{i+1}-\zeta_i)^3} & \zeta_i \le \zeta \le \zeta_{i+1} \\ 6\frac{(\zeta-\zeta_{i-1})^5}{(\zeta_i-\zeta_{i-1})^5} - 15\frac{(\zeta-\zeta_{i-1})^4}{(\zeta_i-\zeta_{i-1})^4} + 10\frac{(\zeta-\zeta_{i-1})^3}{(\zeta_i-\zeta_{i-1})^3} & \zeta_{i-1} \le \zeta \le \zeta_i \\ 0 \qquad\qquad \text{otherwise} \end{cases}$$

$$\bar{Q}_i(\zeta) = \begin{cases} 3\frac{(\zeta_{i+1}-\zeta)^5}{(\zeta_{i+1}-\zeta_i)^4} - 7\frac{(\zeta_{i+1}-\zeta)^4}{(\zeta_{i+1}-\zeta_i)^3} + 4\frac{(\zeta_{i+1}-\zeta)^3}{(\zeta_{i+1}-\zeta_i)^2} & \zeta_i \le \zeta \le \zeta_{i+1} \\ -3\frac{(\zeta-\zeta_{i-1})^5}{(\zeta_i-\zeta_{i-1})^4} + 7\frac{(\zeta-\zeta_{i-1})^4}{(\zeta_i-\zeta_{i-1})^3} - 4\frac{(\zeta-\zeta_{i-1})^3}{(\zeta_i-\zeta_{i-1})^2} & \zeta_{i-1} \le \zeta \le \zeta_i \\ 0 \quad \text{otherwise} \end{cases}$$

$$\bar{\bar{Q}}_i(\zeta) = \begin{cases} 0.5\frac{(\zeta_{i+1}-\zeta)^5}{(\zeta_{i+1}-\zeta_i)^3} - \frac{(\zeta_{i+1}-\zeta)^4}{(\zeta_{i+1}-\zeta_i)^2} + 0.5\frac{(\zeta_{i+1}-\zeta)^3}{(\zeta_{i+1}-\zeta_i)} & \zeta_i \le \zeta \le \zeta_{i+1} \\ 0.5\frac{(\zeta-\zeta_{i-1})^5}{(\zeta_i-\zeta_{i-1})^3} - \frac{(\zeta-\zeta_{i-1})^4}{(\zeta_i-\zeta_{i-1})^2} + 0.5\frac{(\zeta-\zeta_{i-1})^3}{(\zeta_i-\zeta_{i-1})} & \zeta_{i-1} \le \zeta \le \zeta_i \\ 0 \quad \text{otherwise} \end{cases} \tag{3.1}$$

In order to implement the collocation, the Hermite splines within each sub-domain I_γ are mapped onto the interval [0, 1] using a linear mapping $\xi = \dfrac{\zeta - \zeta_{\gamma-1}}{h}$. This linear map reduces the structure of splines mentioned in (3.1) to the tabular form given in Table (1) for $0 \le \xi \le 1$.

Table 1. The Hermite splines and the derivatives for approximation.

i	H_i	$H_i^{(1)}$	$H_i^{(2)}$
1	$1 - 10\xi^3 + 15\xi^4 - 6\xi^5$	$-30\xi^2 + 60\xi^3 - 30\xi^4$	$-60\xi + 180\xi^2 - 120\xi^3$
2	$h(\xi - 6\xi^3 + 8\xi^4 - 3\xi^5)$	$h(1 - 18\xi^2 + 32\xi^3 - 15\xi^4)$	$h(-36\xi + 96\xi^2 - 60\xi^3)$
3	$\frac{h^2}{2}(\xi^2 - 3\xi^3 + 3\xi^4 - \xi^5)$	$\frac{h^2}{2}(2\xi - 9\xi^2 + 12\xi^3 - 5\xi^4)$	$\frac{h^2}{2}(2 - 18\xi + 36\xi^2 - 20\xi^3)$
4	$\frac{h^2}{2}(\xi^3 - 2\xi^4 + \xi^5)$	$\frac{h^2}{2}(3\xi^2 - 8\xi^3 + 5\xi^4)$	$\frac{h^2}{2}(6\xi - 24\xi^2 + 20\xi^3)$
5	$10\xi^3 - 15\xi^4 + 6\xi^5$	$30\xi^2 - 60\xi^3 + 30\xi^4$	$60\xi - 180\xi^2 + 120\xi^3$
6	$h(-4\xi^3 + 7\xi^4 - 3\xi^5)$	$h(-12\xi^2 + 28\xi^3 - 15\xi^4)$	$h(-24\xi + 84\xi^2 - 60\xi^3)$

The Hermite spline collocation method is applied to both the functions u^n, w^n simultaneously. Thus, assuming the following piecewise approximations:

$$u^n(\xi) = \sum_{i=1}^{6} a_i^{\gamma,n} H_i(\xi) \tag{3.2}$$

$$w^n(\xi) = \sum_{k=1}^{6} b_k^{\gamma,n} H_k(\xi) \tag{3.3}$$

where $a^{\gamma_i,n}$,$b^{\gamma_k,n}$ are the controlling constant coefficients to be determined. To implement the orthogonal collocation, the roots of orthogonal polynomials are taken as collocation points within each sub-domain. Traditionally, the zeros of Jacobi polynomials are taken as collocation points. The zeros of Chebyshev or Legendre polynomials of degree six, which are special cases of Jacobi polynomials, are usually chosen as collocation points. In the present study, the zeros of shifted Legendre polynomials of degree six have been taken as collocation points [43]. Using the piecewise approximations defined in Eqs (3.2) and (3.3) in the semi-discretized coupled Eqs (2.5) and (2.6), the following system of equations is obtained:

$$\sum_{i=1}^{6} b_i^{\gamma,n+1} H_i(\xi) + \frac{1}{h^2}\sum_{i=1}^{6} a_i^{\gamma,n+1} H_i^{(2)}(\xi) = -\sum_{i=1}^{6} b_i^{\gamma,n} H_i(\xi) - \frac{1}{h^2}\sum_{i=1}^{6} a_i^{\gamma,n} H_i^{(2)}(\xi) \tag{3.4}$$

$$\sum_{i=1}^{6} a_i^{\gamma,n+1} H_i(\xi) - \frac{\kappa\tau}{2} \sum_{i=1}^{6} b_i^{\gamma,n+1} H_i(\xi) - \frac{\tau}{2h}\alpha(\sum_{i=1}^{6} a_i^{\gamma,n+1} H_i(\xi)) \left\{ \sum_{i=1}^{6} a_i^{\gamma,n} H_i^{(1)}(\xi) \right\}$$
$$-\frac{\tau}{2h} \sum_{i=1}^{6} a_i^{\gamma,n+1} H_i^{(1)}(\xi)\alpha(\left\{ \sum_{i=1}^{6} a_i^{\gamma,n} H_i(\xi) \right\}) - \frac{\delta\tau}{2h} \sum_{i=1}^{6} b_i^{\gamma,n+1} H_i^{(1)}(\xi) - \frac{\varepsilon\tau}{2h^2} \sum_{i=1}^{6} b_i^{\gamma,n+1} H_i^{(2)}(\xi)$$
$$= \sum_{i=1}^{6} a_i^{\gamma,n} H_i(\xi) + \frac{\kappa\tau}{2} \sum_{i=1}^{6} b_i^{\gamma,n} H_i(\xi) + \frac{\delta\tau}{2h} \sum_{i=1}^{6} b_i^{\gamma,n} H_i^{(1)}(\xi) + \frac{\varepsilon\tau}{2h^2} \sum_{i=1}^{6} b_i^{\gamma,n} H_i^{(2)}(\xi) \tag{3.5}$$

The matrix formulation of the algebraic system of Eqs (3.4) and (3.5) can be represented in the following form:

$$\mathcal{P}\lambda^{n+1} = \mathcal{Q}\lambda^n \tag{3.6}$$

$$\mathcal{P} = \begin{bmatrix} P_1 & & & & & & \\ & P_2 & & & & & \\ & & \ddots & & & & \\ & & & P_r & & & \\ & & & & \ddots & & \\ & & & & & P_{m-1} & \\ & & & & & & P_m \end{bmatrix}_{8m\times 8m}$$

$$\mathcal{Q} = \begin{bmatrix} Q_1 & & & & & & \\ & Q_2 & & & & & \\ & & \ddots & & & & \\ & & & Q_r & & & \\ & & & & \ddots & & \\ & & & & & Q_{m-1} & \\ & & & & & & Q_m \end{bmatrix}_{8m\times 8m}$$

The structure of each block of the matrices $\mathcal{P}$ and $\mathcal{Q}$ is given below:

$$P_r = \begin{bmatrix} \rho_{ki} & \kappa_{ki} \\ \nu_{ki} & \eta_{ki} \end{bmatrix}_{8\times 12}; Q_r = \begin{bmatrix} \chi_{ki} & \phi_{ki} \\ \psi_{ki} & \alpha_{ki} \end{bmatrix}_{8\times 12}$$

For $r = 1, m$ the order of block P_r and Q_r is 8×10 due the homogeneous boundary constraints. The above components of the matrix blocks are defined as below:

$$\rho_{ki} = H_i(\xi_k),\ \kappa_{ki} = \frac{1}{h^2} H_i^{(2)}(\xi_k),$$
$$\nu_{ki} = H_i(\xi_k) - \frac{6\tau}{2h} H_i(\xi_k)\{\sum_{i=1}^{6} a_l^{\gamma,j} H_i^{(1)}(\xi_k)\} - \frac{6\tau}{2h} H_i^{(1)}(\xi_k)\{\sum_{i=1}^{6} a_l^{\gamma,j} H_i(\xi_k)\},$$
$$\eta_{ki} = -\frac{\tau}{2h} H_i^{(1)}(\xi_k),\ \phi_{ki} = -\frac{1}{h^2} H_i^{(2)}(\xi_k),\ \chi_{ki} = -H_i(\xi_k),\ \psi_{ki} = H_i(\xi_k),\ \alpha_{ki} = \frac{\tau}{2h} H_i^{(1)}(\xi_k)$$

The matrix formulation defined in Eq (3.6) is solved using mathematical software such as MATLAB. With the increment in the order of the algebraic system and decrement in the step size in the time direction, the computational cost increases. In order to balance the computational cost, the optimal choice of partitions has been chosen, and good accuracy is achieved.

4. Stability analysis

In this section, the stability of the proposed technique is discussed using the Von-Neumann criterion of stability. For quasi-linearization, let us assume $\alpha(u)$ is locally bounded by η over the given domain. Therefore, the linearized coupled system reads:

$$w^{j+1} + u_{\zeta\zeta}^{j+1} = -(w^j + u_{\zeta\zeta}^j), \tag{4.1}$$

$$u^{j+1} - \frac{\kappa\tau}{2}w^{j+1} - \frac{\delta\tau}{2}w_{\zeta}^{j+1} - \frac{\varepsilon\tau}{2}w_{\zeta_\zeta}^{j+1} + \frac{\eta\tau}{2}u_{\zeta}^{j+1} = u^j + \frac{\kappa\tau}{2}w^j + \frac{\delta\tau}{2}w_{\zeta}^j + \frac{\varepsilon\tau}{2}w_{\zeta\zeta}^j - \frac{\eta\tau}{2}u_{\zeta}^j. \tag{4.2}$$

In the form of operator, the linearized problem in Eqs (4.1) and (4.2) can be written as

$$\mathcal{T}(u, w)^{j+1} = \mathcal{E}_\tau. \tag{4.3}$$

It is clear from Eq (4.1) that $(w + u_{\zeta\zeta})^{j+1} + (w + u_{\zeta\zeta})^j = 0$; also, initially $(w + u_{\zeta\zeta})^0 = 0$ this implies $(w + u_{\zeta\zeta})^j = 0 \forall j$. Thus, the boundedness of both w and $u_{\zeta\zeta}$ throughout the given domain is ensured. Application of the piecewise Hermite spline collocation technique as discussed in Eqs (3.2) and (3.3), in Eq (4.1), one gets:

$$\sum_{i=1}^{6} H_i(\xi)b_i^{\gamma,j+1} + \sum_{i=1}^{6}\frac{H_i^{(2)}(\xi)}{h^2}a_i^{\gamma,j+1} = -\left(\sum_{i=1}^{6} H_i(\xi)b_i^{\gamma,j} + \sum_{i=1}^{6}\frac{H_i^{(2)}(\xi)}{h^2}a_i^{\gamma,j}\right),$$

$$\implies \sum_{i=1}^{6} H_i(\xi)b_i^{\gamma,j+1} + \sum_{i=1}^{6}\frac{H_i^{(2)}(\xi)}{h^2}a_i^{\gamma,j+1} = 0.$$

Similarly, considering the relation between w and $u_{\zeta\zeta}$, it can be derived that:

$$\sum_{i=1}^{6}\frac{H_i^{(1)}(\xi)}{h}b_i^{\gamma,j+1} + \sum_{i=1}^{6}\frac{H_i^{(3)}(\xi)}{h^3}a_i^{\gamma,j+1} = 0;$$

$$\sum_{i=1}^{6}\frac{H_i^{(2)}(\xi)}{h^2}b_i^{\gamma,j+1} + \sum_{i=1}^{6}\frac{H_i^{(4)}(\xi)}{h^4}a_i^{\gamma,j+1} = 0. \tag{4.4}$$

Again, considering the second equation of the coupled system stated in Eq (4.2), it is simple to say that:

$$\sum_{i=1}^{6} a_i^{\gamma,j+1}H_i(\xi) - \frac{\kappa\tau}{2}\sum_{i=1}^{6} b_i^{\gamma,j+1}H_i(\xi) - \frac{\delta\tau}{2h}\sum_{i=1}^{6} b_i^{\gamma,j+1}H_i^{(1)}(\xi) - \frac{\varepsilon\tau}{2h^2}\sum_{i=1}^{6} b_i^{\gamma,j+1}H_i^{(2)}(\xi)$$

$$+\frac{\eta\tau}{2h}\sum_{i=1}^{6} a_i^{\gamma,j+1}H_i^{(1)}(\xi) = \sum_{i=1}^{6} a_i^{\gamma,j}H_i(\xi) + \frac{\kappa\tau}{2}\sum_{i=1}^{6} b_i^{\gamma,j}H_i(\xi) + \frac{\delta\tau}{2h}\sum_{i=1}^{6} b_i^{\gamma,j}H_i^{(1)}(\xi)$$

$$+\frac{\varepsilon\tau}{2h^2}\sum_{i=1}^{6} b_i^{\gamma,j} H_i^{(2)}(\xi) - \frac{\eta\tau}{2h}\sum_{i=1}^{6} a_i^{\gamma,j} H_i^{(1)}(\xi).$$

Now, using the relations given in Eq (4.4), the following equation is obtained:

$$\sum_{i=1}^{6}\left(H_i(\xi)+\frac{\eta\tau}{2h}H_i^{(1)}(\xi)\right)a_i^{\gamma,j+1}(\xi)+\frac{\kappa\tau}{2h^2}\sum_{i=1}^{6}H_i^{(2)}(\xi)\left(a_i^{\gamma,j+1}+a_i^{\gamma,j}\right)+\frac{\delta\tau}{2h^3}\sum_{i=1}^{6}H_i^{(3)}(\xi)\left(a_i^{\gamma,j+1}+a_i^{\gamma,j}\right)$$
$$+\frac{\varepsilon\tau}{2h^4}\sum_{i=1}^{6}H_i^{(4)}(\xi)\left(a_i^{\gamma,j+1}+a_i^{\gamma,j}\right)=\sum_{i=1}^{6}\left(H_i(\xi)-\frac{\eta\tau}{2h}H_i^{(1)}(\xi)\right)a_i^{\gamma,j}(\xi) \quad (4.5)$$

further rearranging the terms, Eq (4.5) can be written as:

$$\begin{aligned}&\sum_{i=1}^{6}\left(H_i(\xi)+\frac{\eta\tau}{2h}H_i^{(1)}(\xi)+\frac{\kappa\tau}{2h^2}H_i^{(2)}(\xi)+\frac{\delta\tau}{2h^3}H_i^{(3)}(\xi)+\frac{\varepsilon\tau}{2h^4}H_i^{(4)}(\xi)\right)a_i^{\gamma,j+1}\\&=\sum_{i=1}^{6}\left(H_i(\xi)-\frac{\eta\tau}{2h}H_i^{(1)}(\xi)-\frac{\kappa\tau}{2h^2}H_i^{(2)}(\xi)-\frac{\delta\tau}{2h^3}H_i^{(3)}(\xi)-\frac{\varepsilon\tau}{2h^4}H_i^{(4)}(\xi)\right)a_i^{\gamma,j}\end{aligned} \quad (4.6)$$

Now, assume $a_j^{\gamma,n} = \rho^n \exp(i\mu j)$, where μ represents the mode number, ρ is the amplification factor, and $i = \sqrt{-1}$, and substituting in Eq (4.6), one obtains:

$$\sum_{p=1}^{6} M_p(\xi)\rho^{j+1}\exp(ip\mu) = \sum_{p=1}^{6} N_p(\xi)\rho^{j}\exp(ip\mu),$$

where

$$\begin{aligned}M_p(\xi) &= H_p(\xi)+\frac{\eta\tau}{2h}H_p^{(1)}(\xi)+\frac{\kappa\tau}{2h^2}H_p^{(2)}(\xi)+\frac{\delta\tau}{2h^3}H_p^{(3)}(\xi)+\frac{\varepsilon\tau}{2h^4}H_p^{(4)}(\xi),\\N_p(\xi) &= H_p(\xi)-\frac{\eta\tau}{2h}H_p^{(1)}(\xi)-\frac{\kappa\tau}{2h^2}H_p^{(2)}(\xi)-\frac{\delta\tau}{2h^3}H_p^{(3)}(\xi)-\frac{\varepsilon\tau}{2h^4}H_p^{(4)}(\xi).\end{aligned} \quad (4.7)$$

It is clear from the structure of $M_p(\xi)$ and $N_p(\xi)$ that $|N_p(\xi)| \leq |M_p(\xi)|$. Therefore,

$$|\rho| = \left|\frac{\sum_{p=1}^{6} N_p(\xi)\exp(ip\mu)}{\sum_{p=1}^{6} M_p(\xi)\exp(ip\mu)}\right| \leq 1.$$

This implies that the given technique is unconditionally stable.

5. Numerical illustrations

The efficiency of any technique is incomplete if it does not study the error norms. Define the L_2-norm and L_∞-norm as:
$\|u\|_\infty = \max_{\zeta\epsilon\Omega} . |u(\zeta, t_j)|$,

$\|u\|_2 = \sqrt{h\sum_{k=0}^{m} u(\zeta_k, t_j)^2}$.
$\|e\|_\infty = \|u_{num} - u_{exact}\|_\infty$,
$\|e\|_2 = \|u_{num} - u_{exact}\|_2$.
$GRE(t_j) = \frac{\sum_{k=0}^{m}|u_{exact}(\zeta_k,t_j)-u_{num}(\zeta_k,t_j)|}{\sum_{k=1}^{m}|u_{exact}(\zeta_k,t_j)|}$

where e represents the difference between exact and approximate solution, u_{exact} is the exact solution, and u_{num} is the numerical approximation of the proposed problem with quintic Hermite splines. GRE represents the global relative error.

Example 1. *In this test problem, Eq (1.2) having the compact form of solution as:*

$$u(\zeta, t) = 15 - 15(\tanh(c_1(\zeta - k_1 t - \bar{\zeta})) + \tanh^2(c_1(\zeta - k_1 t - \bar{\zeta})) - \tanh^3(c_1(\zeta - k_1 t - \bar{\zeta}))); \qquad (5.1)$$

is considered, where $c_1 = \frac{1}{2}; k_1 = 6; \bar{\zeta} = -10$.

The initial and the boundary conditions to approximate the solution are derived from the equation (5.1). Different values of τ, h have been considered to analyze the problem. Figure 1 represents the graphical behavior of the soliton solution generated by the proposed technique. Figures 2 and 3 represent the exact solution and the absolute error showing the agreement of the approximate solution. Soliton solution behavior at different levels of time is represented in Figure 4, whereas Figures 5 and 6 depict the computed measures of error. The GRE and the $\|e\|_2$ both seem to decrease after $T = 3$, ensuring the accuracy of the solution even after a large number of iterations. Computationally, the error norms and GRE have been considered. In Table 2, the progress of GRE, $\|e\|_2$, and the $\|e\|_\infty$ with respect to time is studied. The effect of technique parameters like τ, m simultaneously on the approximation are represented in the form of GRE, $\|e\|_2$ in Table 3. Considering $\tau = 0.0001$, the behavior of GRE, $\|e\|_2$, and $\|e\|_\infty$ is presented in Table 4. A comparative study of the GRE generated from the technique with other methods is presented in Table 5. Clearly, the generated results are found to be better than the existing ones.

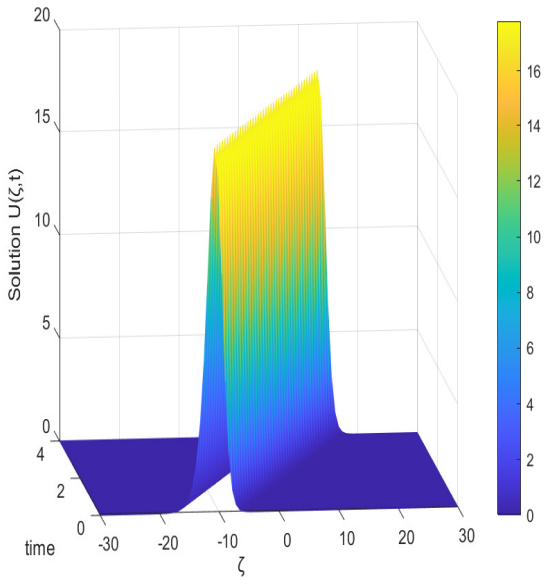

Figure 1. The approximate solution behavior with $\tau = 0.001, m = 100$ up to $T = 4$ for example(1).

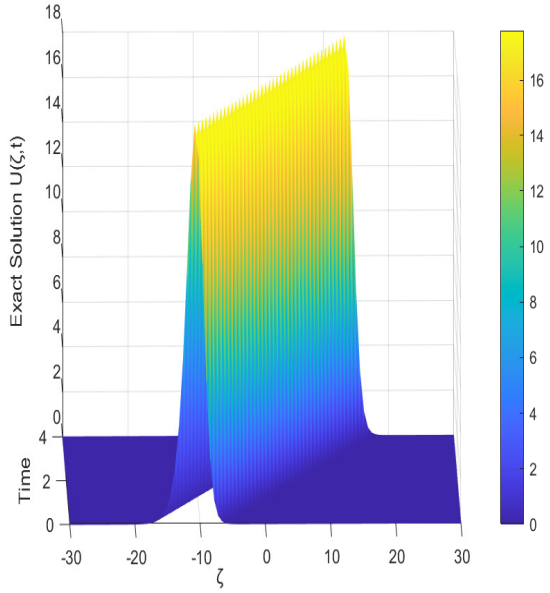

Figure 2. The exact solution behavior for $\tau = 0.001, m = 100$ up to $T = 4$ for example(1).

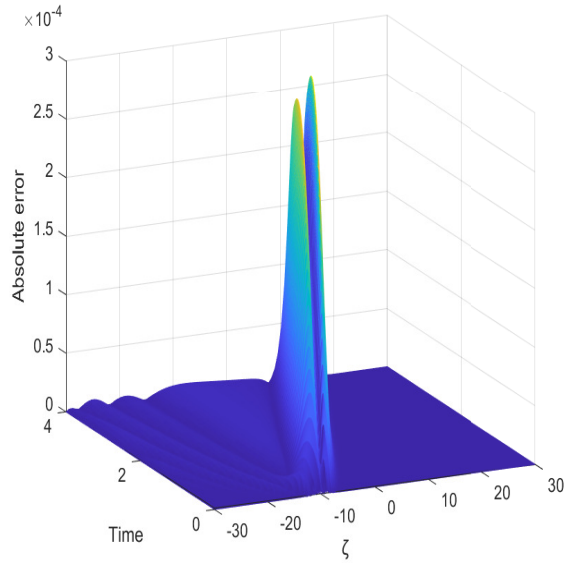

Figure 3. The absolute error with $\tau = 0.001, m = 100$ up to $T = 4$ for example(1).

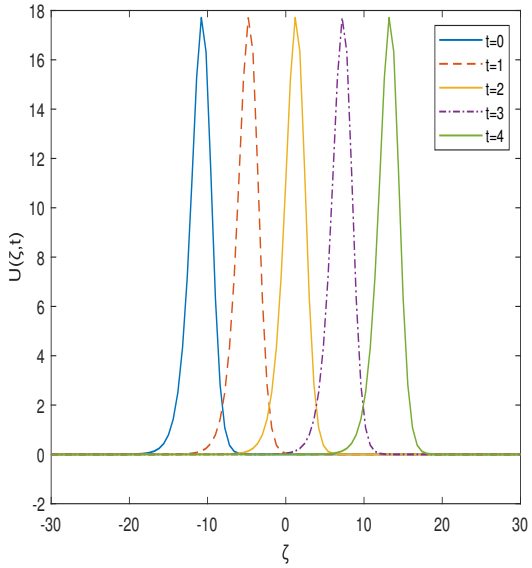

Figure 4. The approximate solution at different time levels with $\tau = 0.001, m = 100$ for example(1).

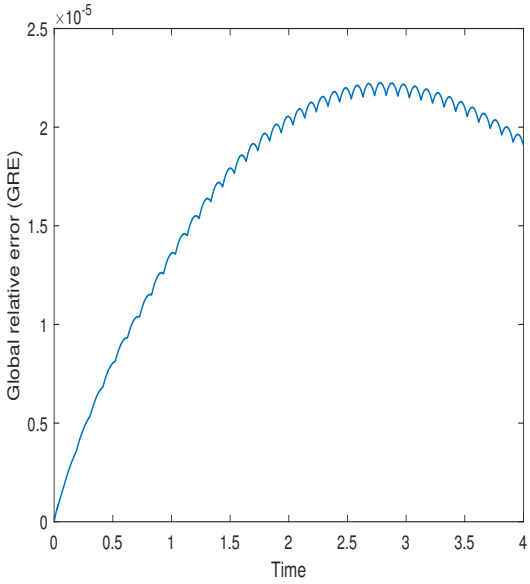

Figure 5. The GRE with $\tau = 0.001, m = 100$ for example(1).

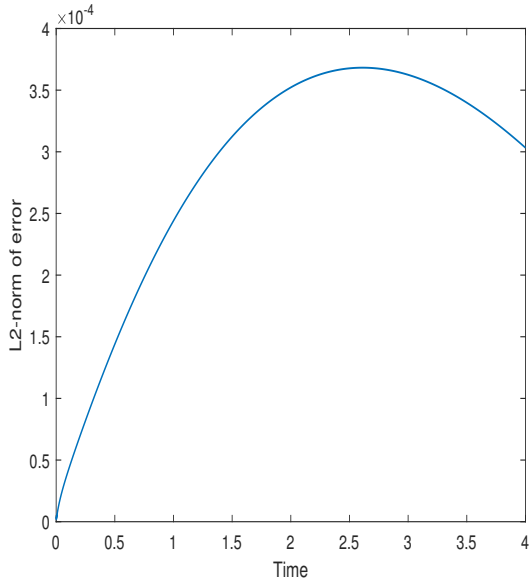

Figure 6. The $||e||_2$ with $\tau = 0.001, m = 100$ for example(1).

Table 2. Behavior of the computed GRE, $||e||_2$, and $||e||_\infty$ with $\tau = 0.001, m = 100$ for example(1).

T	GRE	$\|\|e\|\|_2$	$\|\|e\|\|_\infty$
0.5	8.04313e-06	1.43998e-04	1.22064e-04
1.0	1.36078e-05	2.44052e-04	1.91056e-04
1.5	1.79169e-05	3.12336e-04	2.39644e-04
2.0	2.05323e-05	3.52196e-04	2.65038e-04
2.5	2.19399e-05	3.67707e-04	2.70592e-04
3.0	2.20216e-05	3.62452e-04	2.61325e-04
3.5	2.09862e-05	3.39838e-04	2.50715e-04
4.0	1.90943e-05	3.03281e-04	2.32007e-04

Table 3. Behavior of the computed GRE and $||e||_2$ for different values of τ, m at $T = 1$ example(1).

	$m = 60$		$m = 80$		$m = 100$	
τ	GRE	$\|\|e\|\|_2$	GRE	$\|\|e\|\|_2$	GRE	$\|\|e\|\|_2$
0.01	1.39021e-03	3.14452e-02	1.33659e-03	2.72392e-02	1.36023e-03	2.43602e-02
0.001	1.58780e-05	3.64098e-04	1.35205e-05	2.75786e-04	1.36078e-05	2.44052e-04
0.0001	6.34182e-06	1.12855e-04	5.55149e-07	8.72604e-06	1.82577e-07	3.15424e-06

Table 4. Behavior of the computed GRE, $\|e\|_2$, and $\|e\|_\infty$ for $\tau = 0.0001, m = 80$ at different values T for example(1).

	T=0.2	T=0.4	T=0.6	T=0.8	T=1.0
GRE	3.32031e-07	3.35650e-07	4.81134e-07	5.19877e-07	5.55149e-07
$\|e\|_2$	7.75904e-06	7.59700e-06	8.74719e-06	1.03343e-05	8.72604e-06
$\|e\|_\infty$	6.93918e-06	7.64722e-06	5.88548e-06	8.74518e-06	5.53721e-06

Table 5. Comparative study of the GRE with other methods at $T = 1$ for example(1).

	QHSM	Method in [10]			Method [8]	Method [11]
GRE	5.55149e-07	1.2184e-06	5.5060e-07	6.8261e-04	2.5945e-02	0.4075e-02
(m, τ)	$(80, 0.0001)$		$(121, 0.0001)$		$(600, 0.0001)$	$(600, 0.0001)$

Example 2. *In this test problem, the KdV-Burgers equation corresponding to* $\varepsilon = 0$ *and* $\alpha(u) = u$ *is considered in Eq (1.2), having the compact form of solution as:*

$$u(\zeta, t) = 2\rho + \frac{2\rho}{[1 + \exp(2\gamma(\zeta - \rho t))]^2}; \tag{5.2}$$

where $\gamma = \frac{\kappa}{10\delta}; \rho = \frac{6\kappa^2}{25\delta}$.

For computational purpose, $\kappa = -9 \times 10^{-4}, \delta = 2 \times 10^{-5}$ are chosen. The initial and the boundary conditions to approximate the solution are derived from the Eq (5.2). The problem has been analyzed for different values of τ, h. The shock wave profile of solution has been observed in Figures 7 and 8 for approximate and exact solution up to $T = 200$ with $\tau = 0.1, m = 50$. The absolute error between the approximate and exact solution is shown in Figure 9, which signifies that good accuracy has been achieved in approximation. The progress of shock wave with respect to different levels of time T has been studied in Figure 10, whereas Figures 11 and 12 represents the growth of GRE and the $\|e\|_2$ with respect to time T. In Table 6, the computed behavior of GRE, $\|e\|_2$, and the $\|e\|_\infty$ with respect to time T, choosing $\tau = 0.1, m = 50$ is shown. Comparison of the computed GRE with those available in [10] and [44] has been studied in Table 7. The method proposed by [10] has studied the three values of GRE as shown in Table 7 corresponding to the different technique parameters. Clearly, the approximation is better with the proposed technique as compared to those available in [10] and [44].

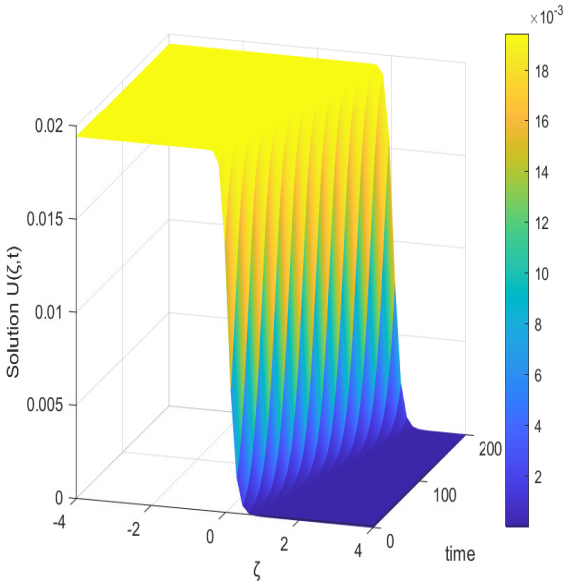

Figure 7. The approximate solution behavior with $\tau = 0.1, m = 50$ up to $T = 200$ for example(2).

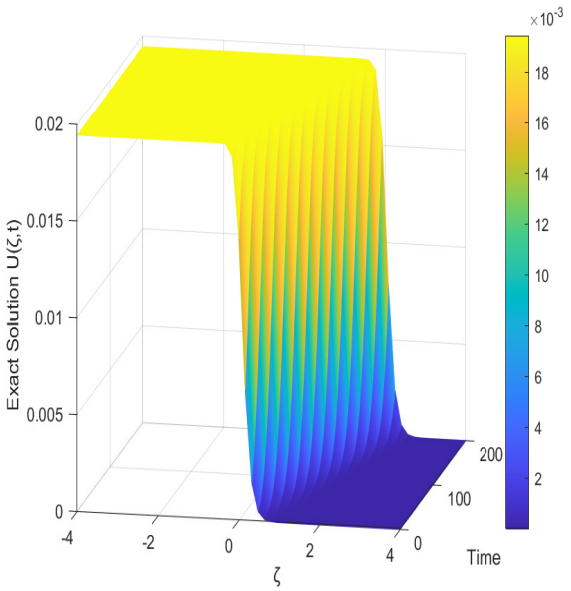

Figure 8. The exact solution behavior with $\tau = 0.1, m = 50$ up to $T = 200$ for example(2).

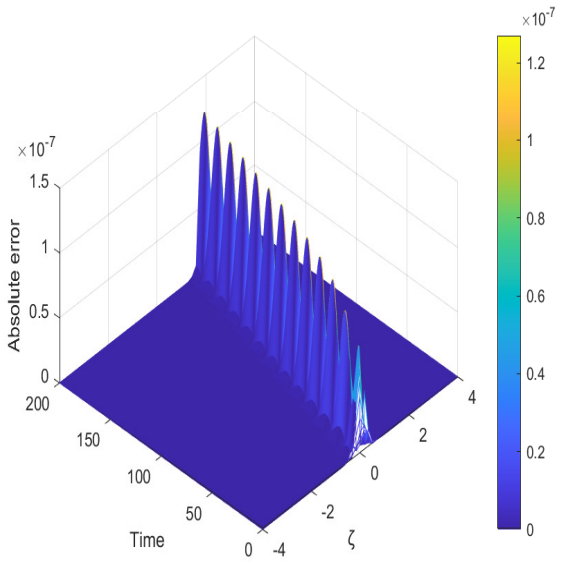

Figure 9. Graphical representation of absolute error with $\tau = 0.1, m = 50$ up to $T = 200$ for example(2).

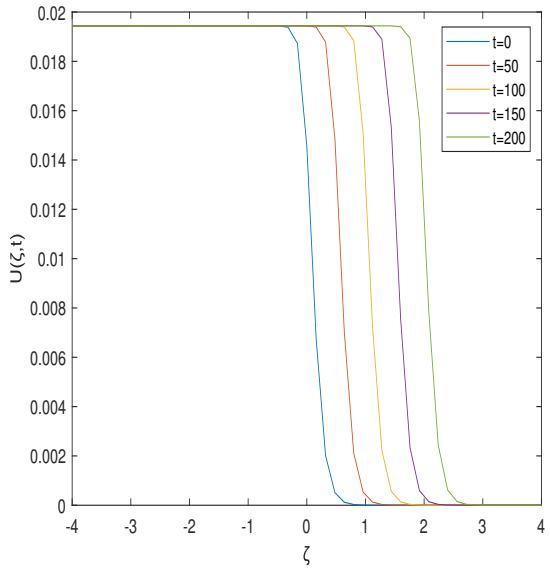

Figure 10. The approximate solution at different time levels with $\tau = 0.1, m = 50$ for example(2).

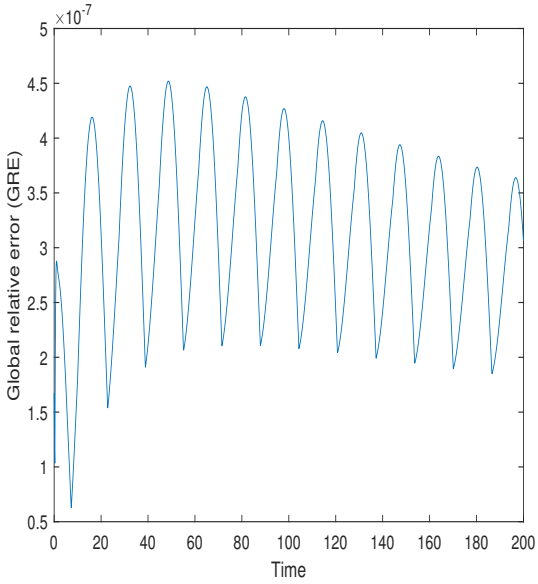

Figure 11. The GRE with $\tau = 0.1, m = 50$ for example(2).

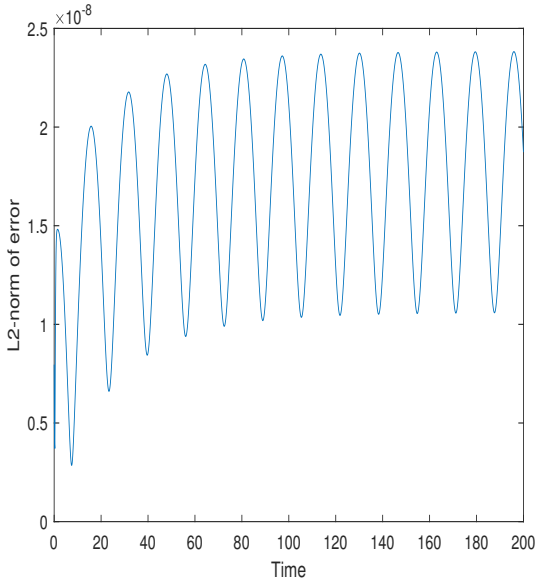

Figure 12. The $||e||_2$ with $\tau = 0.1, m = 50$ for example(2).

Table 6. Variations in the GRE, $||e||_2$ and the $||e||_\infty$ at different time levels with $\tau = 0.1, m = 50$ for example(2).

	$T = 0.0$	$T = 50.0$	$T = 100.0$	$T = 150.0$	$T = 200.0$
GRE	1.67409e-07	4.39441e-07	4.00091e-07	3.52208e-07	3.06519e-07
$\|\|e\|\|_2$	1.45014e-08	2.13959e-08	2.11200e-08	2.00602e-08	1.87295e-08
$\|\|e\|\|_\infty$	7.80192e-08	1.07259e-07	1.06128e-07	1.00410e-07	9.35236e-08

Table 7. Comparative study of the GRE at different time levels for example(2).

Time	QHSM	Method in [10]			Method [44]
50	4.39441e-07	8.143e-06	3.7744e-04	2.7880e-05	9.9928e-05
150	3.52208e-07	1.609e-05	7.5168e-04	6.3142e-05	9.3727e-05
250	2.64658e-07	2.097e-05	8.9492e-04	8.6739e-05	7.5330e-05

Example 3. *In this problem, the Gardner equation as a special case of Eq (1.2) with* $\alpha(u) = u - 5u^2$ *and* $\delta = 1, \varepsilon = 0$ *is considered with the compact form of solution is defined in [45] as:*

$$u(\zeta, t) = \frac{1 - \tanh(l_1(\zeta - \frac{t}{30}))}{10}; \tag{5.3}$$

where $l_1 = \frac{\sqrt{30}}{60}$.

The initial and the boundary conditions are derived from the Eq (5.3). The problem has been studied for different values of τ and h. The kink-type behavior of the solution has been recorded. Figure 13 represents the exact solution, and Figure 14 represents the approximate solution computed with the proposed technique. The agreement of both exact and approximate solutions at the fully discrete temporal-spatial domain is plotted in Figure 15. As can be seen, the approximation accuracy is good. GRE up to $T = 15$ has been plotted in Figure 16. Table 8 compares the GRE and $\|e\|_\infty$ at different time levels with the results given in [45]. For $\tau = 0.001$ and $m = 50$ over the domain $[-50, 50]$, the behavior of GRE, $\|e\|_2$, and $\|e\|_\infty$ with respect to time is shown in Table 9. The effect of τ, m at $T = 1$ on the approximation is studied in Table 10 by GRE, $\|e\|_2$, and the $\|e\|_\infty$. It can be observed that the decrement in τ does not affect the accuracy of approximation very much for this problem, whereas the changes in m, i.e., decrement in h, improve the accuracy.

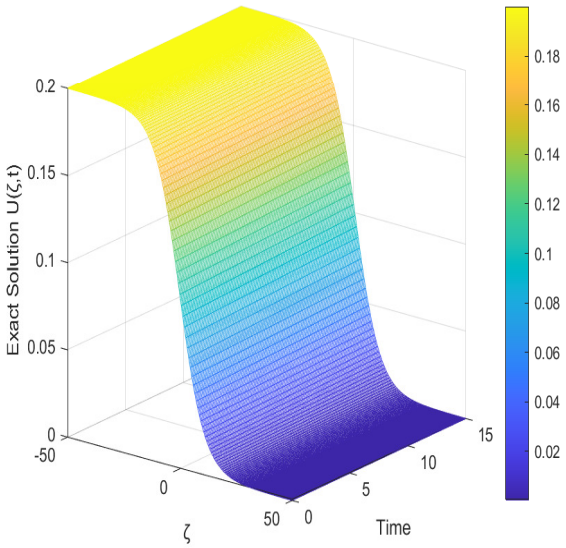

Figure 13. Behavior of exact solution with $\tau = 0.1, m = 150$ up to $T = 15$ for example(3).

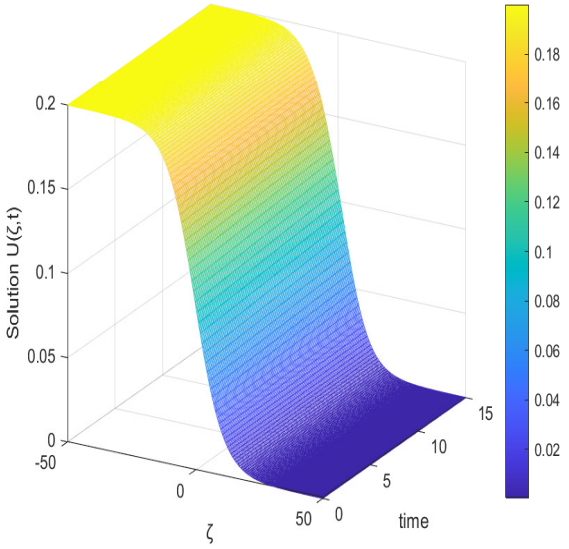

Figure 14. Behavior of approximate solution with $\tau = 0.1, m = 150$ up to $T = 15$ for example(3).

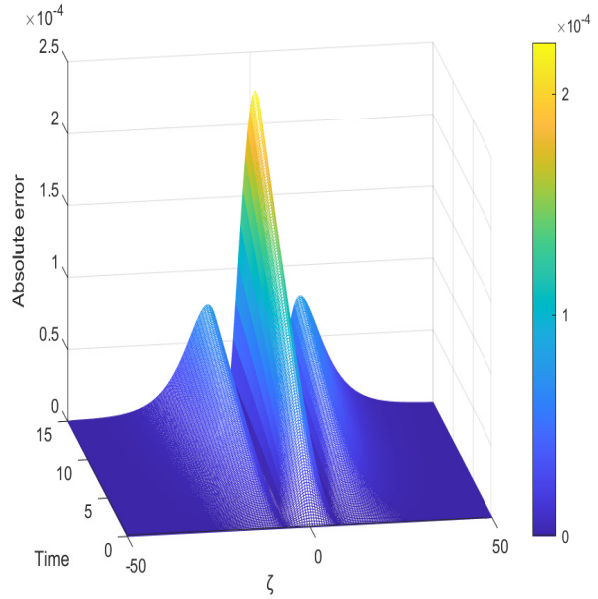

Figure 15. Behavior of absolute error with $\tau = 0.1, m = 150$ up to $T = 15$ for example(3).

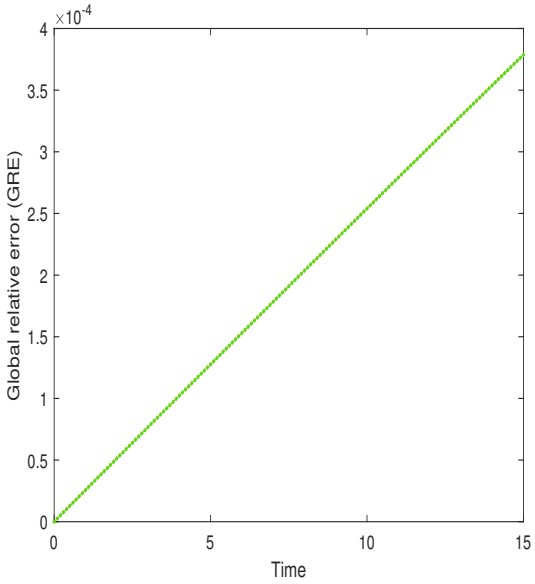

Figure 16. Behavior of GRE with $\tau = 0.1, m = 150$ for example(3).

Table 8. Comparison of the GRE and $\|e\|_\infty$ at different time levels with $\tau = 0.1$ for example(3).

	$(-80, 80), h = 0.1$ [45]		$(-50, 50), h = 2/3$ QHSM	
T	GRE	$\|e\|_\infty$	GRE	$\|e\|_\infty$
0.1	5.1442e–05	2.9570e–05	2.56737e-06	1.54318e-06
0.2	1.0288e–04	5.9142e–05	5.13375e-06	3.08546e-06
0.5	2.5720e–04	1.4786e–04	1.28284e-05	7.70678e-06
1.0	5.1438e–04	2.9575e–04	2.56404e-05	1.53906e-05
2.0	1.0287e–03	5.9159e–04	5.12174e-05	3.06882e-05
5.0	2.5709e–03	1.4796e–03	1.27622e-04	7.60006e-05
10.0	5.1393e–03	2.9610e–03	2.53991e-04	1.50160e-04
15.0	7.7049e–03	4.4434e–03	3.78659e-04	2.23088e-04

Table 9. Comparison of the GRE, $\|e\|_2$, and $\|e\|_\infty$ at different time levels with $\tau = 0.001$ and $m = 50$ over the domain $[-10, 10]$ for example(3).

T	GRE	$\|e\|_2$	$\|e\|_\infty$
0.1	1.03570e-05	4.12075e-06	4.31948e-06
0.2	1.95358e-05	7.12038e-06	6.28697e-06
0.3	2.83276e-05	9.94701e-06	8.06467e-06
0.4	3.68442e-05	1.26925e-05	9.52461e-06
0.5	4.52817e-05	1.53896e-05	1.07819e-05
0.6	5.37134e-05	1.80543e-05	1.18964e-05
0.7	6.20710e-05	2.06954e-05	1.29036e-05
0.8	7.03345e-05	2.33184e-05	1.38266e-05
0.9	7.85132e-05	2.59272e-05	1.46813e-05
1.0	8.66148e-05	2.85242e-05	1.54795e-05

Table 10. Behavior of the computed GRE and $\|e\|_2$ for different values of τ, m at $T = 1$ example(3).

	$\tau = 0.1$		$\tau = 0.01$		$\tau = 0.001$	
m	GRE	$\|e\|_2$	GRE	$\|e\|_2$	GRE	$\|e\|_2$
20	1.04710e-04	5.65792e-05	1.04564e-04	5.64584e-05	1.04558e-04	5.64530e-05
40	9.04729e-05	3.32377e-05	9.04346e-05	3.32206e-05	9.04362e-05	3.32212e-05
60	8.39552e-05	2.53352e-05	8.39589e-05	2.53319e-05	8.39594e-05	2.53320e-05

Example 4. *In this test problem, Eq (1.2) is considered with the following initial function as :*

$$u(\zeta, 0) = \text{sech}^2(\zeta). \tag{5.4}$$

The boundary conditions, in this case, are homogeneous. The problem has been studied for different values of dispersion and dissipation parameters. KdV-Burgers equation for the case $\varepsilon = 0$ has been analyzed for different values of κ, δ. In Figure 17 to Figure 20, the solution behavior has been presented concerning the impact of dispersive and diffusive parameters. Further, the combined effect of dissipative, dispersive, and diffusive parameters has been presented from Figure 21 to Figure 26. It has been observed from Figure 21 to Figure 23 that for $\kappa = \delta = 1$, as the values of ε decrease from 1 to 0.1, more waves arise with rising amplitudes. The simultaneous decrement in the values of dispersive and dissipative parameters has been presented from Figure 24 to Figure 26. The dispersive parameter increases the peaks of the traveling wave. $\|u\|_2$-norm has also been studied corresponding to dissipative, dispersive, and diffusive parameters. In Table 11, $\varepsilon = 0$, i.e., dissipation is zero, with decreasing values of dispersive parameter, a slight decrement in the $\|u\|_2$-norm has been observed, but in the simultaneous decrement in the diffusive and dispersive parameter, the $\|u\|_2$-norm increases as for $\kappa = 0.1, \delta = 0.01$. In Table 12, the effects of dissipation and dispersion parameters are observed. It is observed that with decreasing ε as well as δ, the $\|u\|_2$-norm decreases. The effect of decreasing ε is greater as compared to decreasing δ as for $\kappa = 1, \delta = 1, \varepsilon = 0.1$ and $\kappa = 1, \delta = 0.1, \varepsilon = 0.1$.

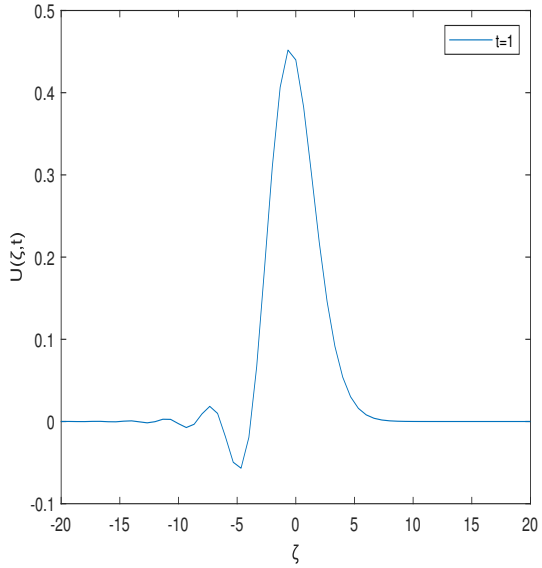

Figure 17. Behavior of solution for KdV-Burgers equation with $\tau = 0.01, m = 60\ \kappa = 1, \delta = 1, \varepsilon = 0$ at $T = 1$ for example(4).

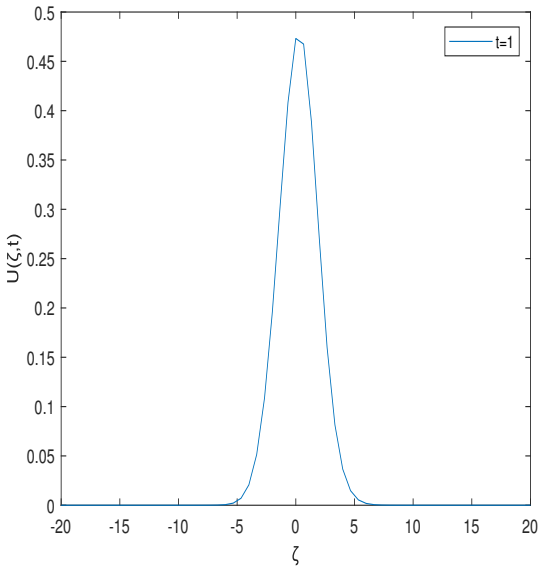

Figure 18. Behavior of solution for KdV-Burgers equation with $\tau = 0.01, m = 60\ \kappa = 1, \delta = 0.1, \varepsilon = 0$ at $T = 1$ for example(4).

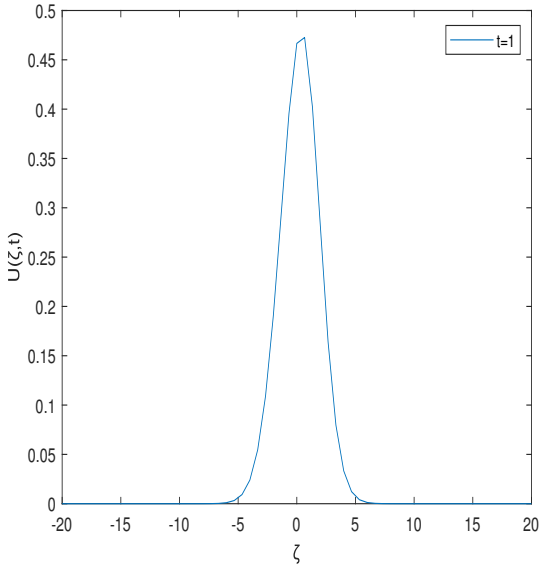

Figure 19. Behavior of solution for KdV-Burgers equation with $\tau = 0.01, m = 60\ \kappa = 1, \delta = 0.01, \varepsilon = 0$ at $T = 1$ for example(4).

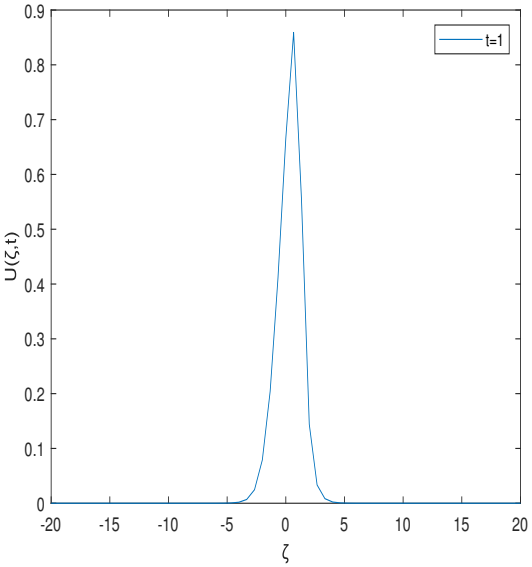

Figure 20. Behavior of solution for KdV-Burgers equation with $\tau = 0.01, m = 60\ \kappa = 0.1, \delta = 0.01, \varepsilon = 0$ at $T = 1$ for example(4).

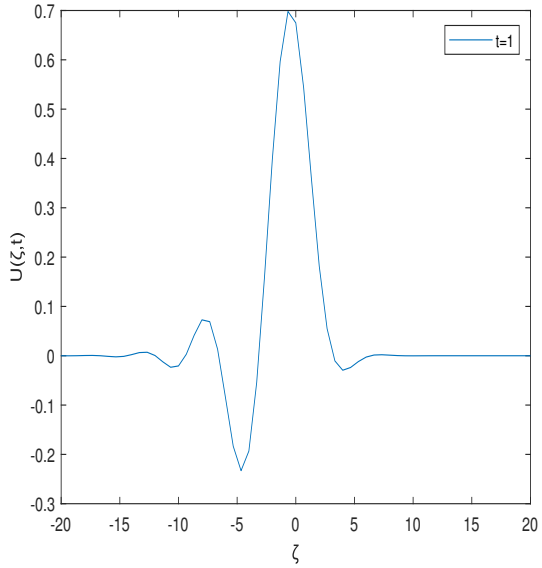

Figure 21. Behavior of solution with $\tau = 0.01, m = 60$ for $\kappa = 1, \delta = 1, \varepsilon = 1$ at $T = 1$ for example(4).

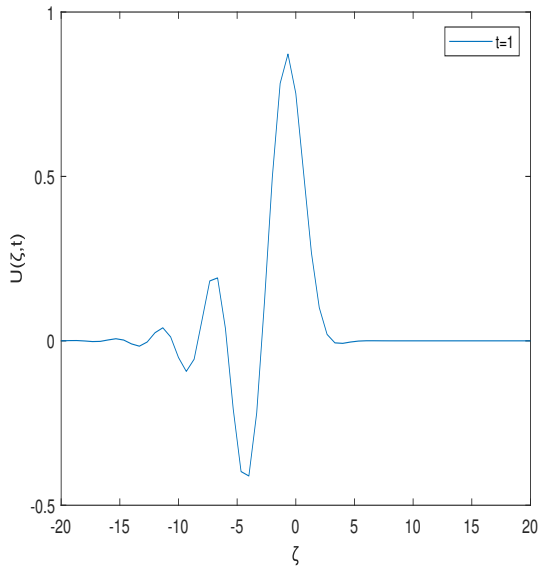

Figure 22. Behavior of solution with $\tau = 0.01, m = 60$ for $\kappa = 1, \delta = 1, \varepsilon = 0.5$ at $T = 1$ for example(4).

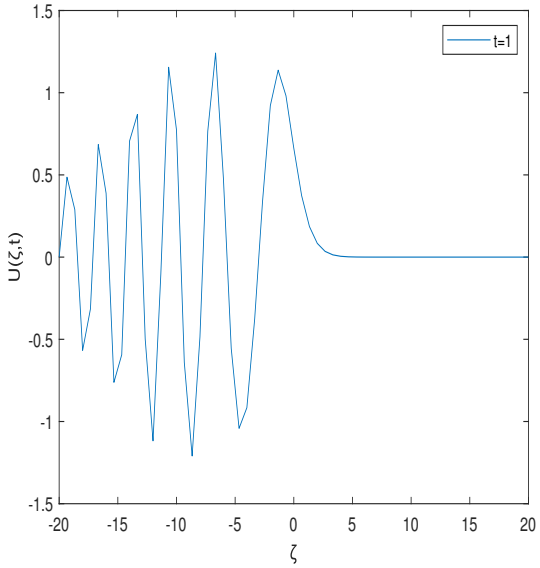

Figure 23. Behavior of solution with $\tau = 0.01, m = 60$ for $\kappa = 1, \delta = 1, \varepsilon = 0.1$ for example(4).

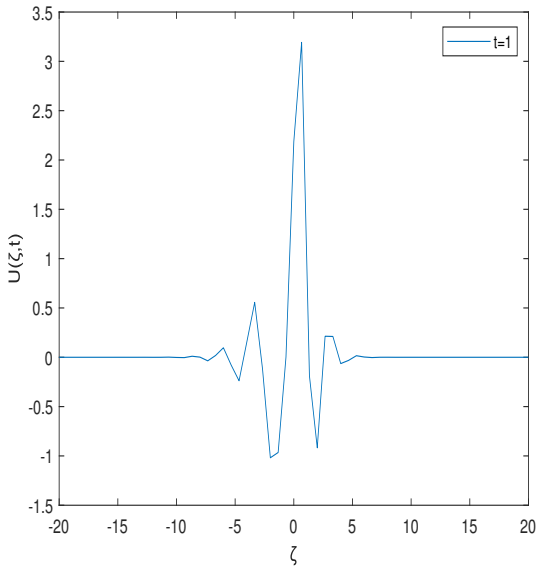

Figure 24. Behavior of solution with $\tau = 0.01, m = 60$ for $\kappa = 1, \delta = 0.1, \varepsilon = 0.1$ at $T = 1$ for example(4).

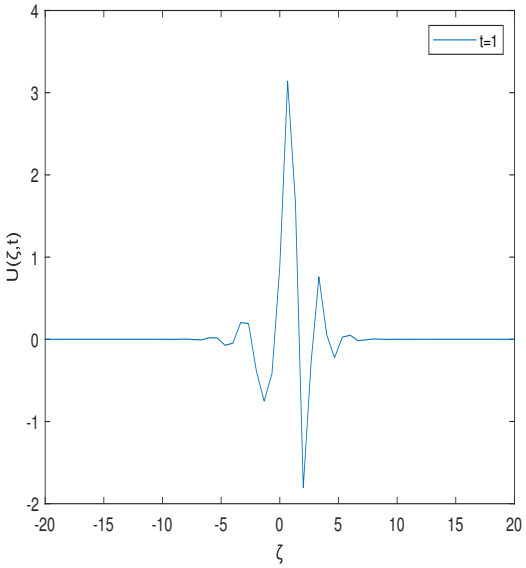

Figure 25. Behavior of solution with $\tau = 0.01, m = 60$ for $\kappa = 1, \delta = 0.01, \varepsilon = 0.1$ at $T = 1$ for example(4).

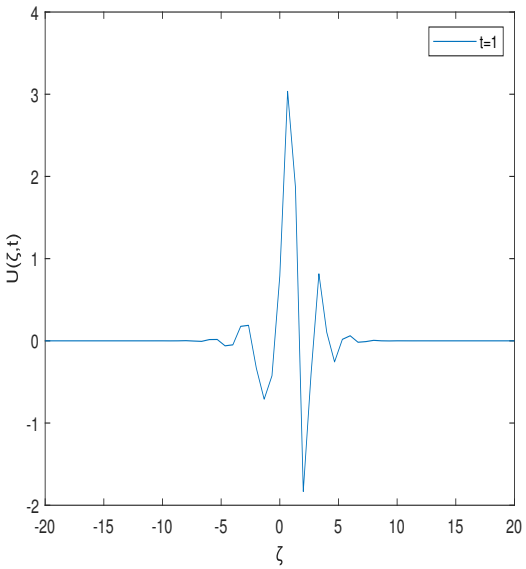

Figure 26. Behavior of solution with $\tau = 0.01, m = 60$ for $\kappa = 1, \delta = 0.001, \varepsilon = 0.1$ at $T = 1$ for example(4).

Table 11. $\|u\|_2$-norm of solution with $\varepsilon = 0, m = 60, \tau = 0.01$ at different time levels corresponding to different values of dispersive and diffusive parameter for Example(4).

T	$\kappa = 1, \delta = 1$	$\kappa = 1, \delta = 0.1$	$\kappa = 1, \delta = 0.01$	$\kappa = 0.1, \delta = 0.01$
0.1	8.40703e-01	8.40328e-01	8.40283e-01	9.04870e-01
0.2	7.90226e-01	7.89165e-01	7.89035e-01	8.96166e-01
0.3	7.52279e-01	7.50564e-01	7.50339e-01	8.88426e-01
0.4	7.22137e-01	7.19875e-01	7.19571e-01	8.81362e-01
0.5	6.97291e-01	6.94586e-01	6.94218e-01	8.74355e-01
0.6	6.76256e-01	6.73194e-01	6.72778e-01	8.66902e-01
0.7	6.58087e-01	6.54735e-01	6.54282e-01	8.58849e-01
0.8	6.42143e-01	6.38557e-01	6.38075e-01	8.50398e-01
0.9	6.27975e-01	6.24197e-01	6.23694e-01	8.41958e-01
1.0	6.15252e-01	6.11318e-01	6.10798e-01	8.33964e-01

Table 12. $\|u\|_2$-norm of solution with $m = 60, \tau = 0.01$ at different time levels corresponding to different values of dissipative, dispersive, and diffusive parameter for Example(4).

T	$\kappa = 1, \delta = 1, \varepsilon = 1$	$\kappa = 1, \delta = 1, \varepsilon = 0.1$	$\kappa = 1, \delta = 0.1, \varepsilon = 0.1$
0.1	8.60531e-01	9.85949e-01	9.85910e-01
0.2	8.50180e-01	1.07531e+00	1.07611e+00
0.3	8.48737e-01	1.18531e+00	1.18951e+00
0.4	8.51420e-01	1.32073e+00	1.33185e+00
0.5	8.56547e-01	1.48838e+00	1.50958e+00
0.6	8.63337e-01	1.69730e+00	1.72957e+00
0.7	8.71363e-01	1.95902e+00	1.99856e+00
0.8	8.80373e-01	2.28594e+00	2.32238e+00
0.9	8.90203e-01	2.69147e+00	2.70449e+00
1.0	9.00744e-01	3.19668e+00	3.14350e+00

Example 5. *In this test problem, the KdV equation is considered as a special case of Eq (1.2) with the initial function as:*

$$u(\zeta, 0) = \text{sech}(\zeta - 1) + \text{sech}(\zeta - 5). \tag{5.5}$$

The problem has been analyzed for the long-time behavior. Also, the effect of domain range has been considered. For time direction, the behavior of the solution from a small time range as in Figure 27 to long-time behavior of the traveling wave as in Figure 30 is examined. For spatial direction, the domain has been extended from $(-10, 10)$ to $(-60, 60)$ and the effect is noticed correspondingly. Different values of τ and m have been considered to analyze the solution for the long-time domain as well as the wider spatial domain. The decreasing wave amplitude has been presented in Figures 28, 29, and 30 for the time and spatial domain. The computed values of $\|u\|_2$-norm are presented in Table 13

and Table 14. The effect of the domain and τ on the $\|u\|_2$-norm at large time levels is studied in Table 13 whereas Table 14 represents the $\|u\|_2$-norm at small time. At the higher times, the $\|u\|_2$-norm seems to decrease irrespective of the domain.

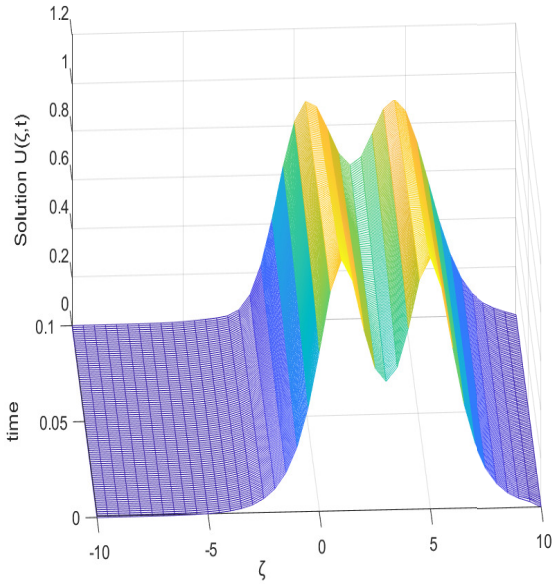

Figure 27. Short time solution behavior of KdV problem with $\tau = 0.001$ for Example(5).

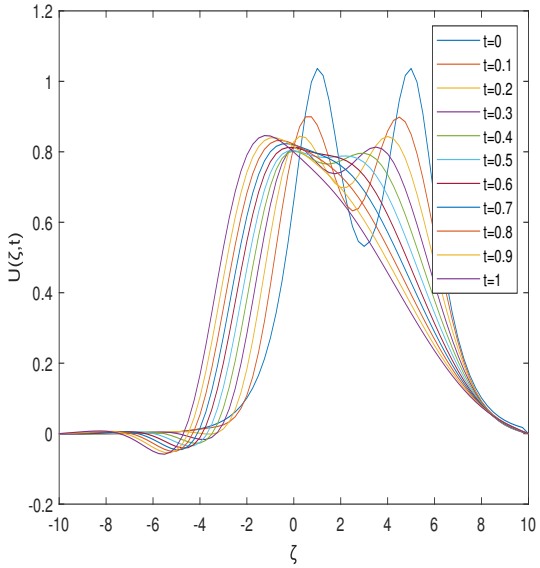

Figure 28. Solution behavior of KdV problem with $\tau = 0.001, m = 80$ for Example(5).

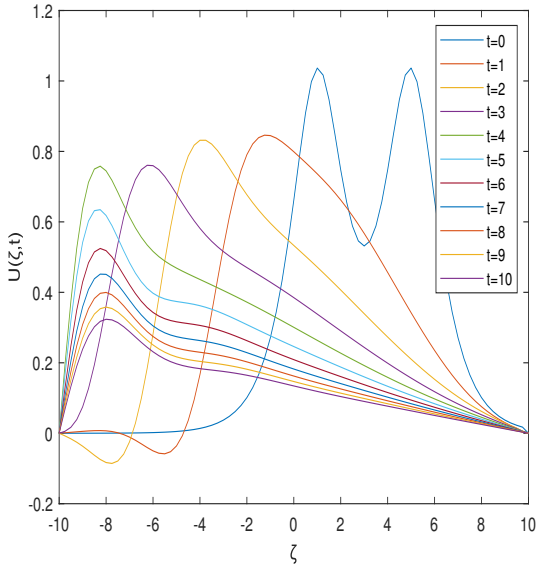

Figure 29. Solution behavior of KdV problem with $\tau = 0.01, m = 80$ for Example(5).

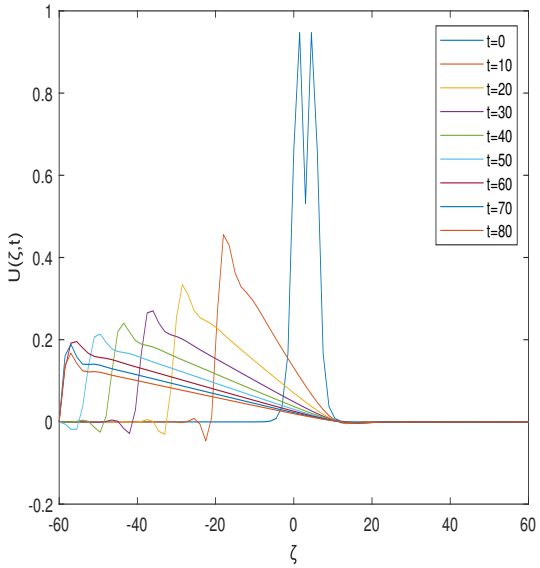

Figure 30. Solution behavior of KdV problem with $\tau = 0.1, m = 120$ for Example(5).

Table 13. Analysis of $\|u\|_2$-norm of solution at large time with respect to different domains and τ for Example(5).

	$[-10, 10]$, $m = 32$		$[-80, 80]$,$m = 120$	
T	$\tau = 0.1$	$\tau = 0.01$	$\tau = 0.1$	$\tau = 0.01$
1.0	1.58154e+00	1.58086e+00	2.30914e+00	2.30864e+00
2.0	1.50089e+00	1.49863e+00	2.19113e+00	2.18786e+00
3.0	1.40173e+00	1.39957e+00	2.05341e+00	2.04994e+00
4.0	1.31101e+00	1.30842e+00	1.93585e+00	1.93317e+00
5.0	1.07170e+00	1.07111e+00	1.84143e+00	1.83951e+00
6.0	9.02970e-01	9.02843e-01	1.76509e+00	1.76372e+00
7.0	7.85945e-01	7.85855e-01	1.70193e+00	1.70094e+00
8.0	6.96921e-01	6.96838e-01	1.64863e+00	1.64789e+00
9.0	6.26110e-01	6.26044e-01	1.60286e+00	1.60230e+00
10.0	5.68453e-01	5.68406e-01	1.56297e+00	1.56254e+00

Table 14. Analysis of $\|u\|_2$-norm of solution at small time with respect to different domains and τ for Example(5).

	$[-10, 10]$, $m = 32$		$[-80, 80]$,$m = 120$	
T	$\tau = 0.1$	$\tau = 0.01$	$\tau = 0.01$	$\tau = 0.001$
0.1	1.65461e+00	1.65459e+00	2.41704e+00	2.41700e+00
0.2	1.63646e+00	1.63644e+00	2.39009e+00	2.39006e+00
0.3	1.62500e+00	1.62498e+00	2.37331e+00	2.37329e+00
0.4	1.61662e+00	1.61661e+00	2.36111e+00	2.36110e+00
0.5	1.60984e+00	1.60983e+00	2.35114e+00	2.35113e+00
0.6	1.60388e+00	1.60388e+00	2.34236e+00	2.34235e+00
0.7	1.59827e+00	1.59827e+00	2.33412e+00	2.33411e+00
0.8	1.59269e+00	1.59269e+00	2.32595e+00	2.32595e+00
0.9	1.58694e+00	1.58693e+00	2.31754e+00	2.31753e+00
1.0	1.58086e+00	1.58086e+00	2.30864e+00	2.30863e+00

6. Conclusions

In this study, higher-order nonlinear dispersive dissipative partial differential equations have been studied. The computational study has been conducted using a hybrid technique comprising a weighted finite difference scheme followed by a collocation method using quintic Hermite splines. The main focus of the present study is toward the traveling wave solution exhibited by the dispersive-dissipative systems. The simultaneous impact of the dispersive-dissipative process, dominating the dispersive process over the dissipative process and vice-versa, has been studied thoroughly.

It is observed that the dominance of dispersion raises the nonlinear waves, whereas the dominance of the dissipative process raises the amplitude of nonlinear waves without dispersion, as studied in Figure 21 to Figure 26. Also, it has been studied that as the dispersion parameter, i.e., δ decreases, the nonlinear waves disappear and make the amplitude higher with the sharp peak, as studied from Figure 24 to Figure 26.

Soliton solution, shock wave solution, and Kink-type solution have also been studied with good approximation accuracy. The stability analysis and the convergence analysis of the adopted technique have also been studied. The computed results show that the applied technique gives fruitful results in studying the traveling wave behavior of nonlinear systems. A comparative study of the computed results with those available in the literature presents the accuracy and efficiency of the technique as well. A good accuracy has been achieved for the small number of partitions in the space as well as in the time direction.

Author contributions

Conceptualization, Shelly Arora and Abdul-Majeed Ayebire; Methodology, Priyanka; Software, Priyanka and Saroj Sahani.

Use of AI tools declaration

The authors declare they have not used Artificial Intelligence (AI) tools in the creation of this article.

Acknowledgments

Dr. Shelly Arora is thankful to SERB-POWER to provide grant to complete this research via grant number SPG/2022/001269. Mr. Abdul Majeed Ayebire is thankful to ICCR for providing grant via reference number LY7930408566174

Conflict of interest

Authors declare that they have no conflict of interest.

References

1. M. Şenol, L. Akinyemi, H. Nkansah, W. Adel, New solutions for four novel generalized nonlinear fractional fifth-order equations, *J. Ocean Eng. Sci.*, (2022). https://doi.org/10.1016/j.joes.2022.03.013
2. M. Richard, W. Zhao, S. Maitama, New analytical modelling of fractional generalized Kuramoto-Sivashinky equation via Atangana-Baleanu operator and J-transform method, *J. Ocean Eng. Sci.*, (2022). https://doi.org/10.1016/j.joes.2022.06.025
3. S. S. Ray, A. K. Gupta, Two-dimensional Legendre wavelet method for travelling wave solutions of time-fractional generalized seventh order KdV equation, *Comput. Math. Appl.*, **73** (2017), 1118–1133. https://doi.org/10.1016/j.camwa.2016.06.046

4. T. J. Bridges, G. Derks, G. Gottwald, Stability and instability of solitary waves of the fifth-order KdV equation: A numerical framework, *Physica D*, **172** (2002), 190–216. https://doi.org/10.1016/S0167-2789(02)00655-3

5. Z. Q. Zhang, H. Ma, A rational spectral method for the KdV equation on the half line, *J. Comput. Appl. Math.*, **230** (2009), 614–625. https://doi.org/10.1016/j.cam.2009.01.025

6. X. Wang, Y. Liu, J. Ouyang, A meshfree collocation method based on moving Taylor polynomial approximation for high order partial differential equations, *Eng. Anal. Bound. Elem.*, **116** (2020), 77–92. https://doi.org/10.1016/j.enganabound.2020.04.002

7. D. Benney, Long waves on liquid films, *J. Math. Phys.*, **45** (1966), 150–155. https://doi.org/10.1002/SAPM1966451150

8. H. Lai, C. Ma, Lattice Boltzmann method for the generalized Kuramoto–Sivashinsky equation, *Physica A*, **388** (2009), 1405–1412. https://doi.org/10.1016/j.physa.2009.01.005

9. M. Lakestani, M. Dehghan, Numerical solutions of the generalized Kuramoto–Sivashinsky equation using B-spline functions, *Appl. Math. Model.*, **36** (2012), 605–617. https://doi.org/10.1016/j.apm.2011.07.028

10. S. Haq, N. Bibi, I. S. Tirmizi, M. Usman, Meshless method of lines for the numerical solution of generalized Kuramoto-Sivashinsky equation, *Appl. Math. Comput.*, **217** (2010), 2404–2413. https://doi.org/10.1016/j.amc.2010.07.041

11. E. Dabboura, H. Sadat, C. Prax, A moving least squares meshless method for solving the generalized Kuramoto-Sivashinsky equation, *Alex. Eng. J.*, **55** (2016), 2783–2787. https://doi.org/10.1016/j.aej.2016.07.024

12. A. H. Khater, R. Temsah, Numerical solutions of the generalized Kuramoto–Sivashinsky equation by Chebyshev spectral collocation methods, *Comput. Math. Appl.*, **56** (2008), 1465–1472. https://doi.org/10.1016/j.camwa.2008.03.013

13. Y. Fu, Z. Liu, Persistence of travelling fronts of KdV–Burgers–Kuramoto equation, *Appl. Math. Comput.*, **216** (2010), 2199–2206. https://doi.org/10.1016/j.amc.2010.03.057

14. A. Mouloud, H. Fellouah, B. A. Wade, M. Kessal, Time discretization and stability regions for dissipative–dispersive Kuramoto–Sivashinsky equation arising in turbulent gas flow over laminar liquid, *J. Comput. Appl. Math.*, **330** (2018), 605–617. https://doi.org/10.1016/j.cam.2017.09.014

15. D. C. Sarocka, A. J. Bernoff, L. F. Rossi, Large-amplitude solutions to the Sivashinsky and Riley–Davis equations for directional solidification, *Physica D*, **127** (1999), 146–176. https://doi.org/10.1016/S0167-2789(98)00281-4

16. J. Daou, A. Kelly, J. Landel, Flame stability under flow-induced anisotropic diffusion and heat loss, *Combust. Flame*, **248** (2023), 112588. https://doi.org/10.1016/j.combustflame.2022.112588

17. M. Benlahsen, G. Bognar, Z. Csati, M. Guedda, K. Hriczo, Dynamical properties of a nonlinear Kuramoto–Sivashinsky growth equation, *Alex. Eng. J.*, **60** (2021), 3419–3427. https://doi.org/10.1016/j.aej.2021.02.003

18. N. A. Kudryashov, Exact solutions of the generalized Kuramoto-Sivashinsky equation, *Phys. Lett. A*, **147** (1990), 287–291. https://doi.org/10.1016/0375-9601(90)90449-X

19. B. Guo, X. Pan, Similarity transformation, the structure of the travelling waves solution and the existence of a global smooth solution to generalized Kuramoto Sivashinsky type equations, *Acta Math. Sci.*, **11** (1991), 48–55. https://doi.org/10.1016/S0252-9602(18)30428-4

20. A. Biswas, D. Swanson, Existence and generalized Gevrey regularity of solutions to the Kuramoto–Sivashinsky equation in R^n, *J. Differ. Equations*, **240** (2007), 145–163. https://doi.org/10.1016/j.jde.2007.05.022

21. Y. Lenbury, C. Rattanakul, D. Li, Stability of solution of Kuramoto-Sivashinsky-Korteweg-de Vries system, *Comput. Math. Appl.*, **52** (2006), 497–508. https://doi.org/10.1016/j.camwa.2005.11.038

22. C. M. Alfaro, R. D. Benguria, M. C. Depassier, Finite mode analysis of the generalized Kuramoto-Sivashinsky equation, *Physica D*, **61** (1992), 1–5. https://doi.org/10.1016/0167-2789(92)90143-B

23. N. A. Kudryashov, On wave structures described by the generalized Kuramoto–Sivashinsky equation, *Appl. Math. Lett.*, **49** (2015), 84–90. https://doi.org/10.1016/j.aml.2015.05.001

24. H. Zhao, S. Tang, Nonlinear stability and optimal decay rate for a multidimensional generalized Kuramoto–Sivashinsky system, *J. Math. Anal. Appl.*, **246** (2000), 423–445. https://doi.org/10.1006/jmaa.2000.6796

25. R. de la Rosa, S. Bruzón, S. María , Symmetry reductions of a generalized Kuramoto–Sivashinsky equation via equivalence transformations, *Commun. Nonlinear Sci.*, **63** (2018), 12–20. https://doi.org/10.1016/j.cnsns.2018.02.038

26. A. P. Hooper, R. Grimshaw, Travelling wave solutions of the Kuramoto-Sivashinsky equation, *Wave Motion*, **10** (1988), 405–420. https://doi.org/10.1016/0165-2125(88)90045-5

27. M. Sajjadian, The shock profile wave propagation of Kuramoto-Sivashinsky equation and solitonic solutions of generalized Kuramoto-Sivashinsky equation, *Acta Univ. Apulensis Math. Inform.*, **38** (2014), 163–176.

28. M. S. Ismail, Numerical solution of complex modified Korteweg-de Vries equation by collocation method, *Commun. Nonlinear Sci.*, **14** (2009), 749–759. https://doi.org/10.1016/j.cnsns.2007.12.005

29. X. Zhang, P. Zhang, A reduced high-order compact finite difference scheme based on proper orthogonal decomposition technique for KdV equation, *Appl. Math. Comput.*, **339** (2018), 535–545. https://doi.org/10.1016/j.amc.2018.07.017

30. M. M. Khader, K. M. Saad, Z. Hammouch, D. Baleanu, A spectral collocation method for solving fractional KdV and KdV-Burgers equations with non-singular kernel derivatives, *Appl. Numer. Math.*, **161** (2021), 137–146. https://doi.org/10.1016/j.apnum.2020.10.024

31. Q. Zhang, L. Liu, Convergence and stability in maximum norms of linearized fourth-order conservative compact scheme for Benjamin–Bona–Mahony–Burgers' equation, *J. Sci. Comput.*, **87** (2021), 1–31. https://doi.org/10.1007/s10915-021-01474-3

32. C. I. Christov, M. G. Velarde, Dissipative solitons, *Physica D*, **86** (1995), 323–347. https://doi.org/10.1016/0167-2789(95)00111-G

33. I. C. Christov, Z. Yu, *Twenty-five years of dissipative solitons*, AIP Conference Proceedings, **2522** 2022. https://doi.org/10.48550/arXiv.2108.13351

34. C. M. Elliott, D. A. French, F. A. Milner, A second order splitting method for the Cahn-Hilliard equation, *Numer. Math.*, **54** (1989), 575–590. https://doi.org/10.1007/BF01396363

35. Priyanka, S. Arora, F. Mebrek-Oudina, S. Sahani, Super convergence analysis of fully discrete Hermite splines to simulate wave behaviour of Kuramoto–Sivashinsky equation, *Wave Motion*, **121** (2023), 103187. https://doi.org/10.1016/j.wavemoti.2023.103187

36. S. Arora, R. Jain, V. K. Kukreja, A robust Hermite spline collocation technique to study generalized Burgers-Huxley equation, generalized Burgers-Fisher equation and Modified Burgers' equation, *J. Ocean Eng. Sci.* (2022). https://doi.org/10.1016/j.joes.2022.05.016

37. S. Arora, R. Jain, V. K. Kukreja, Solution of Benjamin-Bona-Mahony-Burgers equation using collocation method with quintic Hermite splines, *Appl. Numer. Math.*, **154** (2020), 1–16. https://doi.org/10.1016/j.apnum.2020.03.015

38. S. Arora, I. Kaur, Applications of quintic Hermite collocation with time discretization to singularly perturbed problems, *Appl. Math. Comput.*, **316** (2018), 409–421. https://doi.org/10.1016/j.amc.2017.08.040

39. J. Crank, P. Nicolson, *A practical method for numerical evaluation of solutions of partial differential equations of the heat-conduction type*, Mathematical proceedings of the Cambridge philosophical society: Cambridge University Press, **43** (1947), 50–67. https://doi.org/10.1017/S0305004100023197

40. Q. Zhang, Y. Qin, Z. Z. Sun, Linearly compact scheme for 2D Sobolev equation with Burgers' type nonlinearity, *Numer. Algorithms*, **91** (2022), 1081–1114. https://doi.org/10.1007/s11075-022-01293-z

41. Q. Zhang, L. Liu, Z. Zhang, Linearly Implicit Invariant-Preserving Decoupled Difference Scheme For The Rotation-Two-Component Camassa–Holm System, *SIAM J. Sci. Comput.*, **44** (2022), A2226–A2252. https://doi.org/10.1137/21M1452020

42. S. G. Rubin, Jr. Graves, A. Randolph, *A cubic spline approximation for problems in fluid mechanics*, 1975.

43. S. Arora, S. S. Dhaliwal, V. K. Kukreja, Computationally efficient technique for weight functions and effect of orthogonal polynomials on the average, *Appl. math. comput.*, **186** (2007), 623–631. https://doi.org/10.1016/j.amc.2006.08.005

44. Z. Chai, B. Shi, L. Zheng, A unified Lattice Boltzmann model for some nonlinear partial differential equations, *Chaos, Soliton. Fract.*, **36** (2008), 874–882. https://doi.org/10.1016/j.chaos.2006.07.023

45. L. Degon, A. Chowdhury, Approximate solutions to the Gardner equation by spectral modified exponential time differencing method, *Partial Differ. Equ. Appl. Math.*, **5** (2022), 100310. https://doi.org/10.1016/j.padiff.2022.100310

AIMS Press